Supplementary Materials for:

Speleothem sulphate and trace elements constrain Alpine glacial inception across the Marine Isotope Stage 11/10 transition

Jonathan L. Baker[1*], Alexandre Honiat[1], Peter M. Wynn[2], Jens Fohlmeister[3], Martin Trüssel[4], Samuel Hollowood[5], Jiaoyang Ruan[6,7], Regina Mertz-Kraus[8], R. Lawrence Edwards[9], and Christoph Spötl[1]

1. Institute of Geology, Universität Innsbruck, Innrain 52f, 6020 Innsbruck, Austria
2. Lancaster Environment Centre, Lancaster University, Lancaster LA1 4YQ, United Kingdom
3. German Federal Office for Radiation Protection (BfS), Berlin, Germany
4. Foundation Naturerbe Karst und Höhlen Obwalden (NeKO), Alpnach, Switzerland
5. Department of Earth Sciences, University of Oxford, Wellington Square, Oxford OX1 2JD, United Kingdom
6. IBS Center for Climate Physics, Institute for Basic Science, Busan, South Korea
7. State Key Laboratory of Lithospheric and Environmental Coevolution, Institute of Geology and Geophysics, Chinese Academy of Sciences, Beijing, China
8. Institute for Geosciences, Johannes Gutenberg Universität Mainz, Saarstraße 21, 55122 Mainz, Germany
9. Department of Earth Sciences, University of Minnesota, 116 Church St SE, Minneapolis, MN 55455, USA

**Correspondence to*: jonathan.baker@uibk.ac.at

List of Figures and Tables

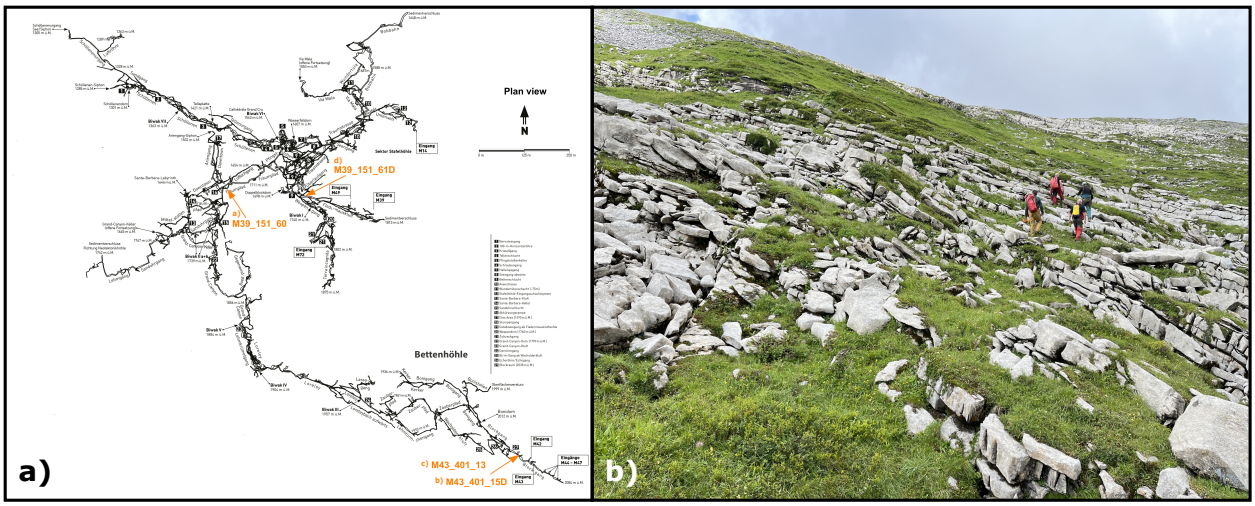

Figure S1: Cave site map and field photo. a) Plan view schematic of Betten Cave (Melchsee Frutt, Switzerland) indicates location of each stalagmite included in the MIS 11–10 composite record. b) Photo of the field area, showing patchy grassy soils near the southern entrance where stalagmites 13 and 15D were collected. View WNW. Map and photo by Martin Trüssel.

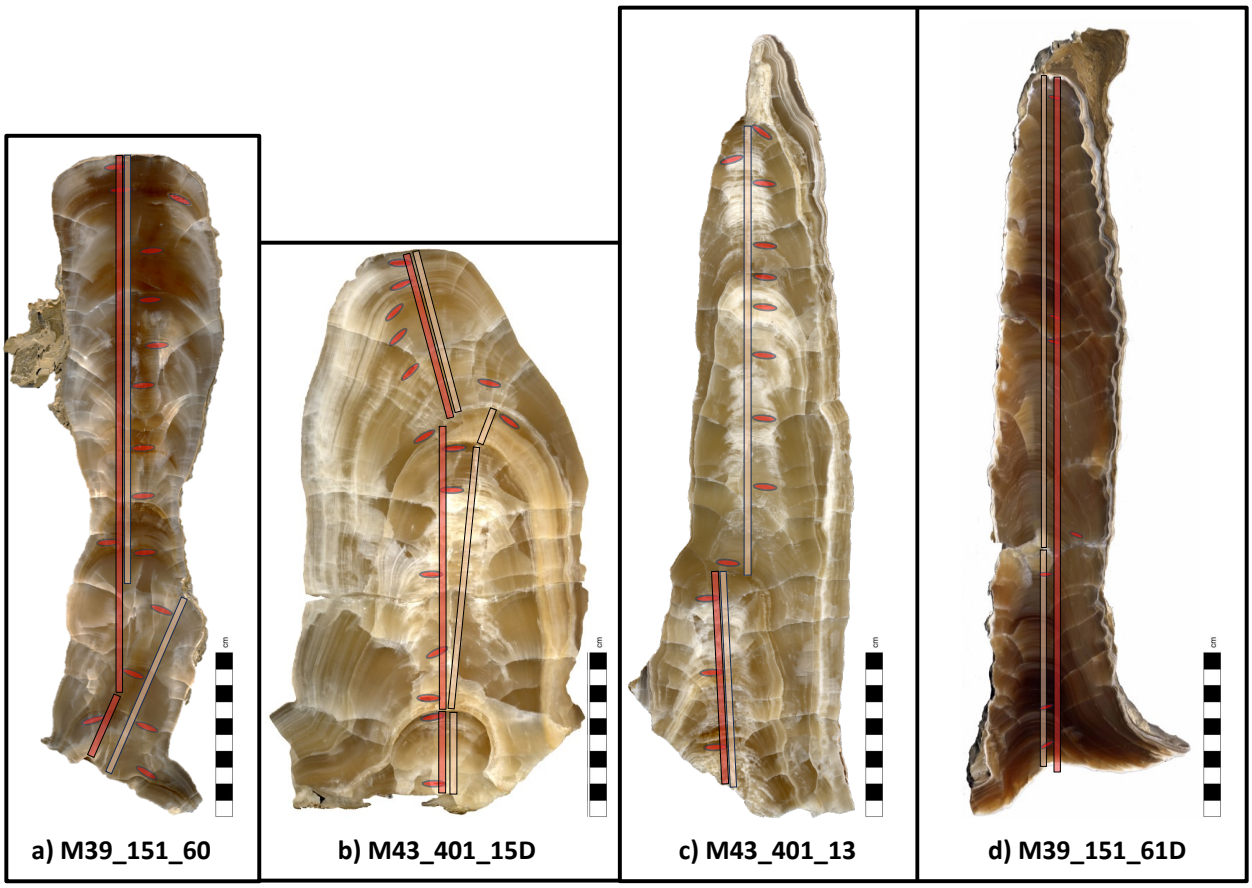

Figure S2: Scan of stalagmite samples with micromill (tan) and LA-ICP-MS (red) tracks.

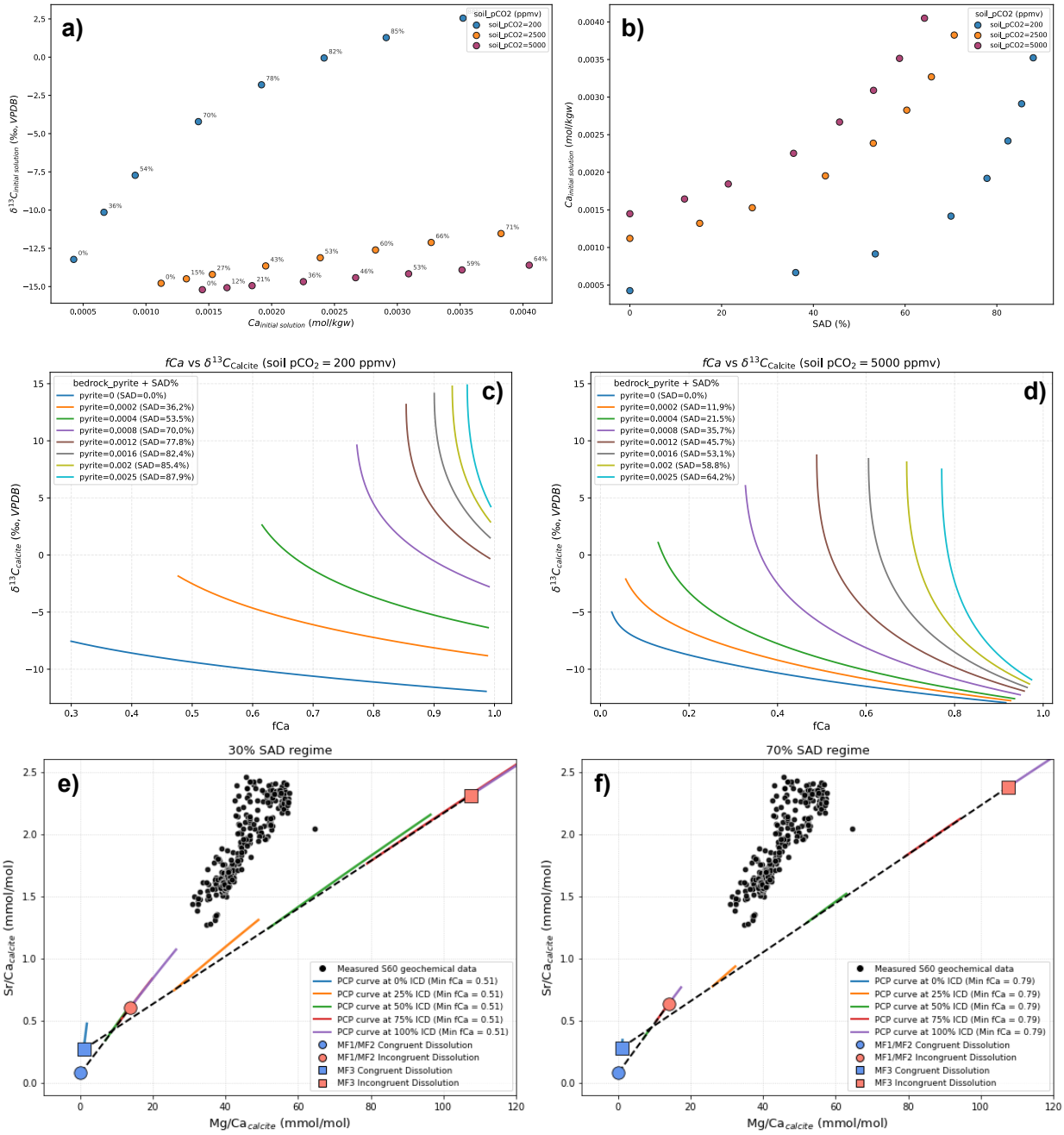

Figure S3: Proxy system modelling experiments in CaveCalc software (Owen et al., 2018). a) Evolution of initial $\delta^{13}C$ of aqueous carbonate as a function of soil pCO_2 and the fraction of sulphuric-acid dissolution (SAD). b) Evolution of initial $[Ca^{2+}]$ as a function of soil pCO_2 and SAD. c) and d) Isotopic (^{13}C) enrichment of calcite in response to prior carbonate precipitation (PCP), quantified as the fraction of initial $[Ca^{2+}]$ remaining in solution at the stalagmite apex (*f*Ca), for increasing contributions from SAD (color-coded enrichment lines). Levels of soil pCO_2 range from (c) the MIS 10 atmosphere (200 ppmv) to (d) a modern-analogue alpine meadow (5000 ppmv). e) and f) Modelling of Mg/Ca and Sr/Ca enrichment from PCP and incongruent calcite dissolution (ICD) of the host rock in a limited SAD (e) and high SAD (f) system. PCP is unable to

replicate the range of Mg/Ca and Sr/Ca concentrations without significant ICD (>50%) of the intercalated marl horizons (MF3). No combination of PCP and ICD can explain speleothem Mg/Ca and Sr/Ca data if the purer limestone member (MF1/MF2) is the only source of minor cations.

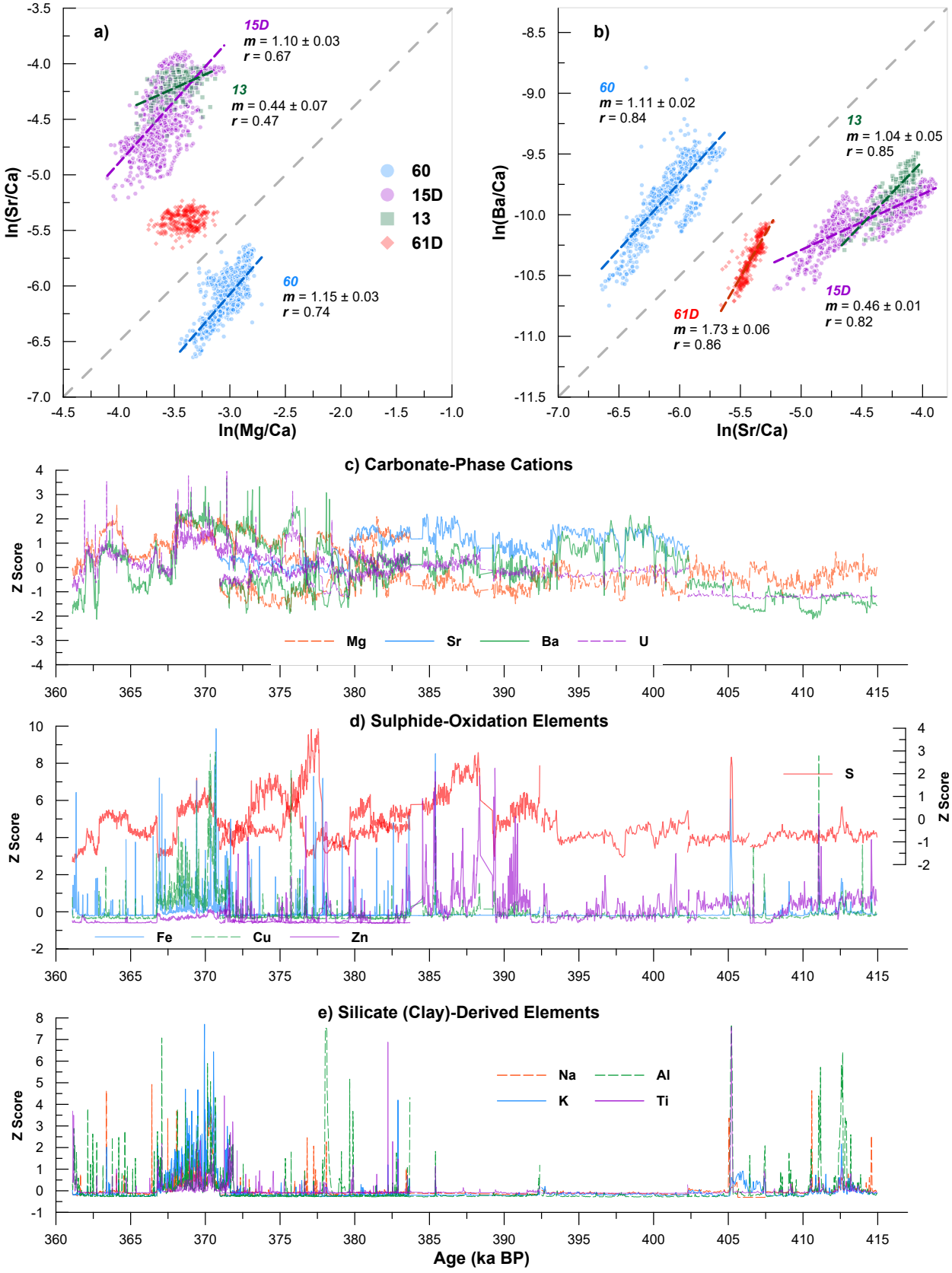
a)
15D
m = 1.10 ± 0.03
r = 0.67
13
m = 0.44 ± 0.07
r = 0.47
60
m = 1.15 ± 0.03
r = 0.74
60
15D
13
61D
ln(Sr/Ca)
ln(Mg/Ca)
b)
60
m = 1.11 ± 0.02
r = 0.84
13
m = 1.04 ± 0.05
r = 0.85
61D
m = 1.73 ± 0.06
r = 0.86
15D
m = 0.46 ± 0.01
r = 0.82
ln(Ba/Ca)
ln(Sr/Ca)
c) Carbonate-Phase Cations
Z Score
Mg
Sr
Ba
U
d) Sulphide-Oxidation Elements
Z Score
S
Z Score
Fe
Cu
Zn
e) Silicate (Clay)-Derived Elements
Z Score
Na
Al
K
Ti
Age (ka BP)

Figure S4: Summary of trace-element data. Classic 'Sinclair Tests' for PCP and ICD controls on Mg/Ca vs. Sr/Ca (a) and Sr/Ca vs. Ba/Ca (b) (Sinclair, 2011; Wassenburg et al., 2024). Least-squares linear regressions yield slopes consistent with these processes for most samples, but the relationship is most clearly expressed in stalagmite 60 from MIS 10, interpreted as subglacial. c) Standardised time series of minor cations from carbonate dissolution: Mg, Sr, Ba, and U. d) Standardised time series of elements potentially associated with sulphide oxidation: S, Fe, Cu, and Zn. e) Standardised time series of elements common to silicate minerals, especially clay minerals found in host rock MF3.

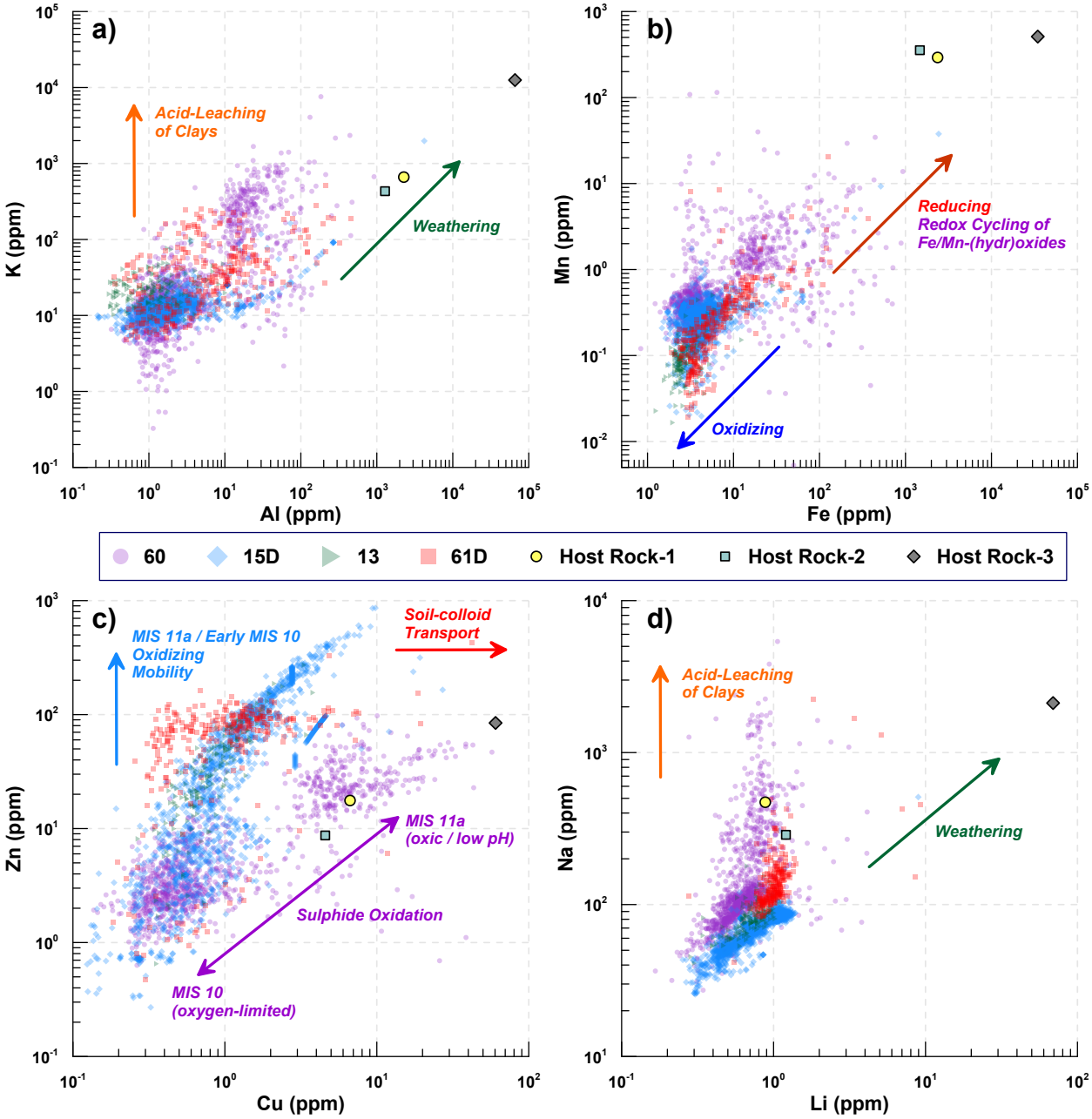

Figure S5: Cross correlation and mixing plots between the host rock and the characteristically low concentrations of 'detrital' elements (normally excluded from the solution and crystal lattice) in clean-calcite speleothems. a) Clay-derived K and Al are typically transported in colloids, but acidic conditions from sulphide oxidation can highly mobilize both elements. Concentrations of K above the mixing line, found in stalagmite 60 after ~372 ka, reflect the acid leaching of clays, which mobilizes K over Al due to cation exchange. b) Redox-sensitive Fe and Mn are (im)mobile in reducing (oxidizing) conditions, but both are introduced to the aquifer via sulphide oxidation. We interpret high values in stalagmite 60 after ~372 ka to reflect remobilization through reductive dissolution of Fe and Mn (oxyhydr)oxides. c) Redox sensitive Cu and Zn are similarly mobilized by sulphide oxidation, but in soil settings, Cu exhibits a higher affinity to organic colloids. d) Na

and Li are common indicators of siliciclastic detritus. Both exhibit mixing-line behaviour with the host rock, but Na (like K) is notably enriched above the mixing line in stalagmite 60 after ~372 ka. We interpret this enrichment to result from the acid leaching of clays, occurring in tandem with the colloidal transport of both elements.

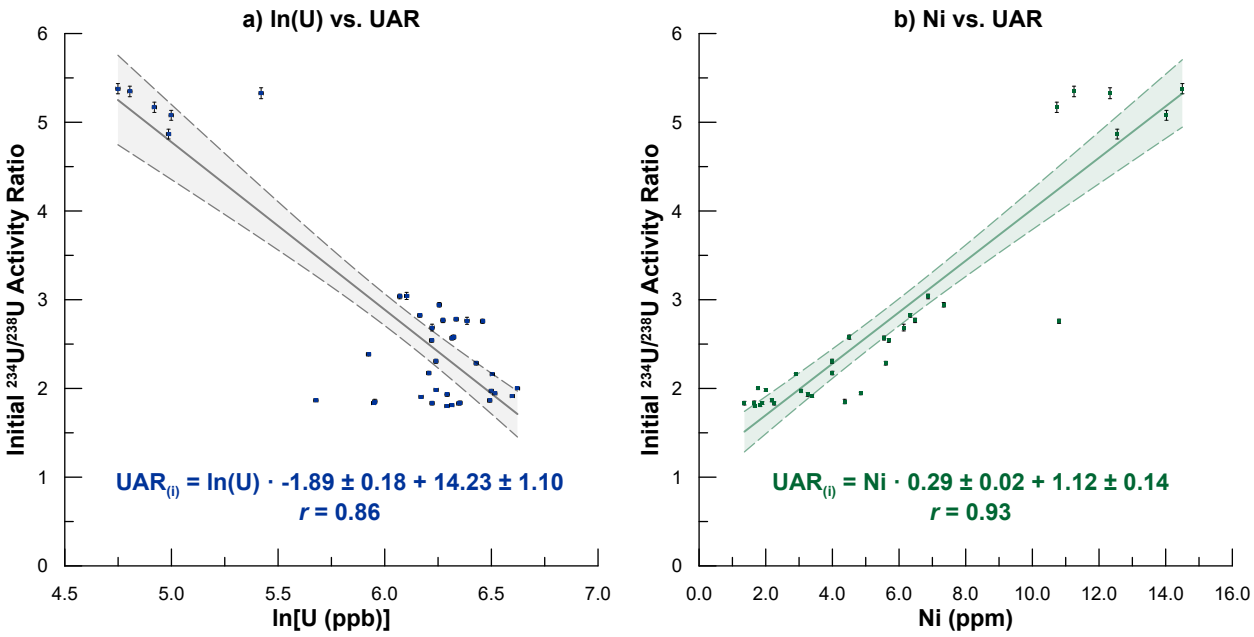

Figure S6: Uranium-isotope systematics in the context of redox-sensitive elements U and Ni. a) Correlation between the natural logarithm of U concentration (in ng/g calcite) and initial UAR. b) Correlation between Ni concentration (in µg/g calcite) and initial UAR. Shading of linear regressions shows 95% confidence interval. Uranium Activity Ratio (UAR) = 1 + ($\delta^{234}U_{(i)}$ / 1000).

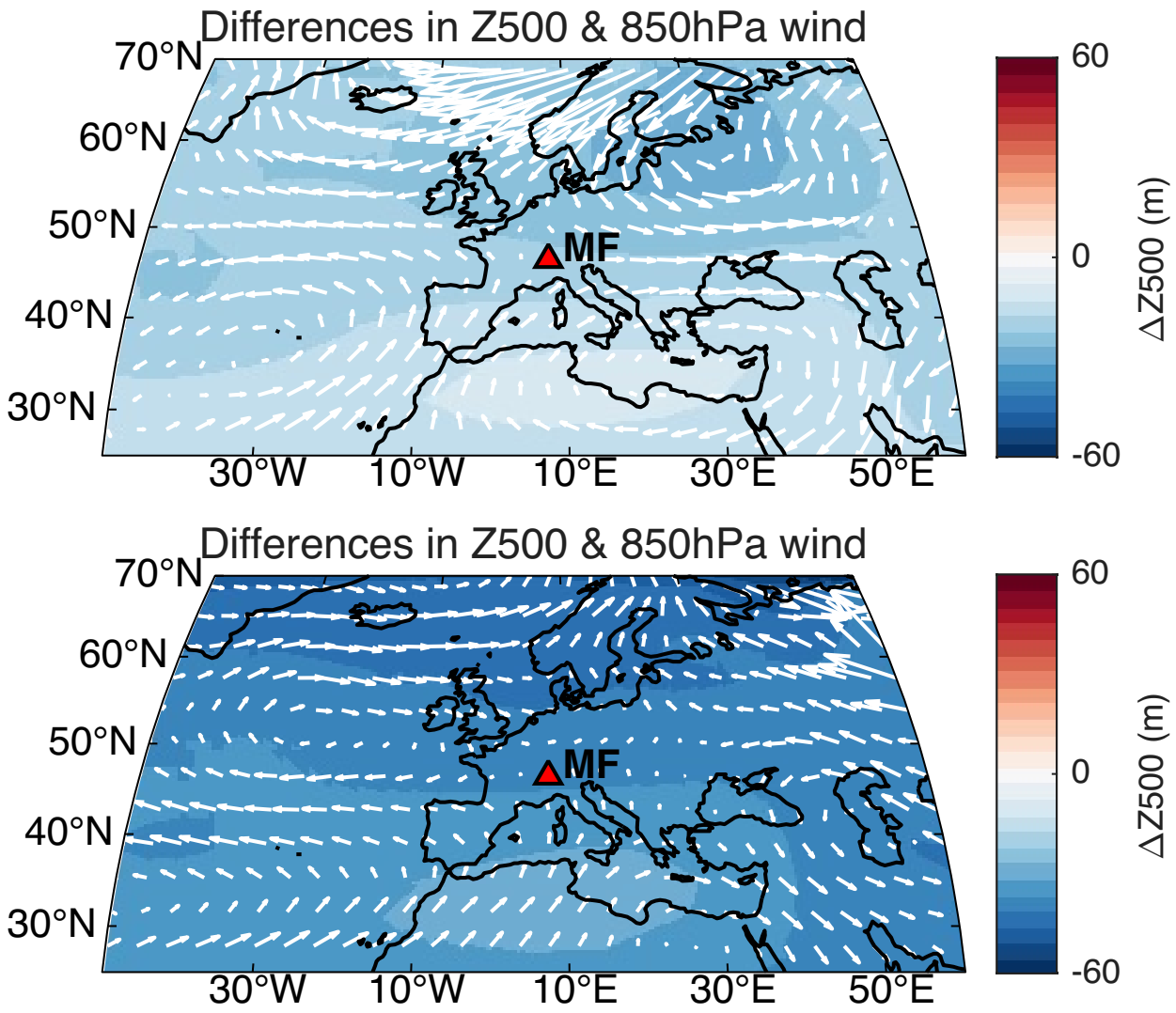

Figure S7: Difference plots of 500-mb geopotential height and 850-mb wind vectors in the transient Community Earth System Model version 1.2 (CESM1.2) simulation (Timmermann et al., 2022; Yun et al., 2023) between environmental stages. a) Anomalies at 380–400 ka vs. 405–415 ka. b) Anomalies at 360–370 ka vs. 380–400 ka. The fully coupled atmosphere–ocean–land–sea ice model was run at ~3.8° horizontal resolution with monthly output and forced by time-varying orbital parameters, greenhouse gas concentrations and prescribed ice-sheet boundary conditions consistent with late Middle Pleistocene climate evolution. Differences in 500 hPa geopotential height and 850 hPa wind vectors were estimated by subtracting the means of three intervals plotted.

References Cited

Sinclair, D.J., 2011. Two mathematical models of Mg and Sr partitioning into solution during incongruent calcite dissolution. Chem. Geol. 283, 119–133. https://doi.org/10.1016/j.chemgeo.2010.05.022

Timmermann, A., Yun, K.S., Raia, P., Ruan, J., Mondanaro, A., Zeller, E., Zollikofer, C., Ponce de León, M., Lemmon, D., Willeit, M., Ganopolski, A., 2022. Climate effects on archaic human habitats and species successions. Nature 604, 495–501. https://doi.org/10.1038/s41586-022-04600-9

Wassenburg, J.A., Samanta, A., Sha, L., Lee, H., Scholz, D., Cheng, H., Stoll, B., Ait Brahim, Y., Budsky, A., Breitenbach, S.F.M., 2024. Trace element partitioning controls on cave drip water compositions through prior calcite and aragonite precipitation. Commun. Earth Environ. 5, 488. https://doi.org/10.1038/s43247-024-01648-5

Yun, K.-S., Timmermann, A., Lee, S.-S., Willeit, M., Ganopolski, A., Jadhav, J., 2023. A transient coupled general circulation model (CGCM) simulation of the past 3 million years. Climate of the Past 19, 1951–1974. https://doi.org/10.5194/cp-19-1951-2023